Talanta 99 (2012) 256–261

Contents lists available at SciVerse ScienceDirect

Talanta

journal homepage: www.elsevier.com/locate/talanta

Nanocomposites of palladium nanoparticle-loaded mesoporous carbon nanospheres for the electrochemical determination of hydrogen peroxide

Xiaojun Bian [a], Kai Guo [a], Lei Liao [a], Jingjing Xiao [a], Jilie Kong [a], Chang Ji [b], Baohong Liu [a,*]

[a] Department of Chemistry, State Key Lab of Molecular Engineering of Polymer and Institute of Biomedical Sciences, Fudan University, Shanghai 200433, China
[b] Department of Chemistry and Biochemistry, Texas State University, San Marcos, TX 78666, USA

ARTICLE INFO

Article history:
Received 24 February 2012
Received in revised form
18 May 2012
Accepted 22 May 2012
Available online 29 May 2012

Keywords:
Electrochemical sensor
Mesoporous carbon nanospheres
Palladium nanoparticles
Hydrogen peroxide

ABSTRACT

Palladium nanoparticles (Pd NPs) were loaded in situ on novel mesoporous carbon nanospheres (MCNs), which possess high specific surface area and large pore volume. The resulting Pd/MCNs hybrid nanocomposites were characterized by X-ray diffraction (XRD) and transmission electron microscopy (TEM). By using Pd/MCNs as the catalyst matrices to modify the surface of glassy carbon electrode, a nonenzymatic sensor was developed for the determination of hydrogen peroxide (H_2O_2). Cyclic voltammetry (CV) and amperometry (at an applied potential of −0.30 V versus SCE) were used to study and optimize the performance of the electrochemical sensor. It was demonstrated that the sensor not only exhibits good electrocatalytic activity toward the reduction of H_2O_2 but also has high sensitivity (307.5 μA mM^{-1} cm^{-2}), low detection limit of 1.0 μM, and wide linear response range from 7.5 μM to 10 mM. Moreover, the sensor shows excellent stability and anti-interference capability for the detection of H_2O_2.

1. Introduction

Hydrogen peroxide (H_2O_2) is an essential substance that needs to be frequently analyzed in industry, clinic, and environment [1–3]. It is also a major by-product of many biological reactions catalyzed by various enzymes such as glucose oxidase and horseradish peroxidase [4]. The rapid and reliable determination of H_2O_2 is of great importance and many approaches have been used to measure the H_2O_2 concentration including titrimetry [5], chemiluminescence [6], fluorescence [7], spectrophotometry [8], and electrochemical analysis [9,10]. Among these techniques, the electrochemical sensors have attracted significant interests and have become promising tools for the detection of H_2O_2 due to their simplicity, low cost, fast response, high selectivity and sensitivity, low detection limit, and ease of miniaturization. The method is usually based upon the surface modification of electrodes with enzymes or proteins (e.g. cytochrome *c* [10], myoglobin [11,12], hemoglobin [13], or horseradish peroxidase [14]), which can accelerate the electron transfer between the electrodes and H_2O_2. Nevertheless, enzyme-modified electrodes often show low stability and require complex immobilization procedures and critical operation conditions. These disadvantages can greatly limit their applications in the practical analysis of H_2O_2. To address such issues, attempts have been made to detect H_2O_2 by sensors without the involvement of enzymes [15–17]. The nonenzymatic H_2O_2 sensors generally rely on the direct current response from the reduction or oxidation of H_2O_2 at the electrode surface to function properly. Consequently, the appropriate modification of electrode surface becomes increasingly important in order to enhance the electron transfer between the electrode and H_2O_2 as well as to minimize the overpotential.

More recently, numerous unique nanocompounds have provided new opportunities for the development of novel nonenzymatic H_2O_2 sensors. Among the various nanomaterials, the three-dimensional (3D) ordered mesoporous carbons have inspired considerable research interests due to their distinctive properties and great potentials of being applied as catalyst supports [18,19], electrode materials [20,21], adsorbents [22], energy storage media [23,24], and templates for the preparation of other nanostructured inorganic substances [25,26]. Their combined features of high specific surface areas and ordered channels can significantly decrease the resistance of substances transferring through the channels as well as allow a higher dispersion and loading of the catalysts and more efficient diffusion of the reagents. In light of this, 3D ordered mesoporous carbon materials, especially the spherical particles, are ideal candidates for catalyst supports [27]. On the other hand, noble metal nanoparticles (NPs) have also attracted extensive attentions for their applications in many aspects including SERS [28,29], catalysis [30], and biosensoring [31]. Among the noble metal NPs, palladium NPs are of particular interest as they have excellent catalytic activities in hydrogenation or Heck coupling reaction [32,33],

* Corresponding author. Tel.: +86 21 65642405; fax: +86 21 65641740.
E-mail address: bhliu@fudan.edu.cn (B. Liu).

0039-9140/$ - see front matter © 2012 Elsevier B.V. All rights reserved.
http://dx.doi.org/10.1016/j.talanta.2012.05.048

electrooxidation of formic acid [34,35], oxygen reduction in fuel cells [36,37], and detection of vital analytes (e.g., H_2O_2, glucose, NADH, and hydrazine) which usually undergo sluggish electrochemical redox processes [38–42].

In this work, Pd NPs were loaded in situ on the novel mesoporous carbon nanospheres (MCNs), which have a high specific surface area of 719 $m^2\ g^{-1}$, a volume capacity of 0.98 $cm^3\ g^{-1}$, and uniform mesoporous channels of approximately 3 nm in diameter. The hybrid Pd/MCNs nanocomposites were characterized by transmission electron microscopy (TEM) and X-ray diffraction (XRD). Furthermore, the Pd/MCNs modified glassy carbon electrode (GCE) was fabricated for the determination of H_2O_2 via electrochemical reduction by using cyclic voltammetric (CV) and amperometric methods. The studies showed that the nonenzymatic H_2O_2 sensor has high sensitivity and selectivity, low detection limit, wide linear range, and good stability.

2. Experimental section

2.1. Reagents

Triblock copolymer Pluronic F127 ($PEO_{106}PPO_{70}PEO_{106}$, M.W. 12,600), $PdCl_2$, and Nafion® perfluorinated ion-exchange resin solution (5% w/w) were purchased from Sigma-Aldrich. NH_4F, H_3BO_3, $NaBH_4$, H_2O_2 aqueous solution (30% w/w), phenol, formalin aqueous solution (37% w/w), ammonia, and anhydrous ethanol were obtained from Shanghai Chemical Plant. Stock solutions of H_2O_2 were freshly prepared prior to the measurements. The phosphate buffer solutions (PBS, pH = 7.0) were made by sodium phosphates (molar ratio of Na_2HPO_4:NaH_2PO_4 is 62:38). All reagents were of analytical grade and double distilled water was used in the experiments.

2.2. Synthesis of nanomaterials

Mesoporous carbon nanospheres (MCNs) were prepared according to Zhao's method [43]. Briefly, 0.30 g of phenol, 1.05 mL of formalin aqueous solution, and 7.5 mL of 0.10 M NaOH aqueous solution were mixed and stirred at 70 °C for 0.5 h. Afterwards, 0.48 g of triblock copolymer Pluronic F127 was dissolved in 7.5 mL of distilled water and added to the mixture, which was further stirred at 66 °C for 2 h. Additional 25 mL of water was added subsequently to dilute the solution, followed by stirring for another 18 h. After being cooled down, 17.7 mL of the solution and 56 mL of water were transferred into an autoclave and kept at 130 °C for 24 h. The mixture was centrifuged, washed with copious amount of water, and dried at 50 °C overnight. The final products were obtained after carbonization at 700 °C under nitrogen atmosphere for 3 h. Prior to use, MCNs were sonicated in a mixture of concentrated HNO_3 and H_2SO_4 (1:3 in volume ratio) for 4 h. The treated MCNs were washed with copious distilled water, centrifuged, and dried in oven.

Hybrid Pd/MCNs were prepared according to the literature with some modifications [41]. First, 10.7 mg of NH_4F, 43.4 mg of H_3BO_3, and 1.05 mL of 0.045 M $PdCl_2$ solution were mixed with 10 mL of distilled water. Subsequently, 20 mg of MCNs was dispersed into the solution by ultrasonication. After the pH was adjusted to between 8 and 9 by using concentrated ammonia, 5.0 mL of 0.030 M $NaBH_4$ was slowly added with vigorous stirring. Another 8 h of stirring were carried out to complete the reaction. Finally, the products were collected by filtration, washed with water, and dried under vacuum at 60 °C.

2.3. Characterization of materials

Nitrogen adsorption/desorption isotherm was collected by Quantachrome's Quadrasorb SI analyzer at 77 K. Prior to measurements, the samples were degassed at 523 K for 3 h under vacuum. The specific surface area and pore size distribution were calculated by the Brunauer–Emmet–Teller (BET) and density functional theory (DFT) methods, respectively. X-ray diffraction (XRD) pattern was recorded with the aid of Bruker D8 advanced X-ray diffractometer using the Ni-filtered Cu Kα radiation at a wavelength of 0.154 nm (40 mV working voltage and 40 mA working current). The hybrid Pd/MCNs were pressed and loaded onto the sample plate to collect the XRD pattern, which was analyzed by the Bruker DIFFRAC-XRD Commander software. TEM images were obtained by a JEOL JEM-2011 electron microscope at an acceleration voltage of 200 kV. Thermogravimetric analysis (TGA) was carried out by Pyris 1 TGA instrument under air atmosphere at a heating rate of 10 °C/min from 25 to 700 °C.

2.4. Electrode preparation and electrochemical analysis

The glassy carbon electrode (GCE, 3.5 mm in diameter) was polished sequentially with 1, 0.3, and 0.05 μm alumina slurry and sonicated in ethanol and distilled water before being dried in a stream of nitrogen gas. The Pd/MCNs catalyst powder (2.0 mg) was dispersed in 1.0 mL of a solution composed of distilled water and ethanol (4:1 in volume ratio) containing 100 μL of Nafion, followed by ultrasonication to form a homogeneous slurry. Nafion was used for the purpose of forming a stable Pd/MCNs membrane on the GCE electrode surface and reducing the interferences from anions for the sensor in a certain pH range [44]. Subsequently, 8 μL of the catalyst slurry was pipetted and spread on the glassy carbon electrode surface and dried under infrared light. The Pd/MCNs modified GCE (Pd/MCNs-GCE) was used as the working electrode for the electrochemical studies. CV and amperometry were carried out in N_2 saturated phosphate buffer solution (20 mM, pH = 7.0) at room temperature by a CHI 660C electrochemical workstation (Chenhua Instrument Co., Shanghai, China). A conventional three-electrode setup was employed using a Pd/MCNs-GCE working electrode, a saturated calomel reference electrode (SCE), and a platinum foil counter electrode.

3. Results and discussion

3.1. Characterization of hybrid Pd/MCNs nanocomposites

Fig. 1 shows the nitrogen adsorption/desorption isotherm and pore size distribution (inset) of MCNs. It was found that the MCNs have a large specific surface area of 719 $m^2\ g^{-1}$, a pore volume of 0.98 $cm^3\ g^{-1}$, and narrow pore size of approximately 3 nm in diameter. These properties could favor a better dispersion and loading of metal NPs on and within the MCNs, which would be the ideal catalyst supports. In addition, surface functionalization of carbon materials is believed to be critical for loading of metal NPs [9,15]. Prior to acidification, the MCNs surface is hydrophobic, which is not favorable for the accommodation of the water soluble Pd^{2+}. With the treatment by a mixture of concentrated HNO_3 and H_2SO_4, the MCNs surface will become more hydrophilic and ideal for the preparation of hybrid Pd/MCNs nanocomposites.

Fig. 2a and b show the TEM images of the MCNs after acidification and the hybrid Pd/MCNs, respectively. The treated MCNs (Fig. 2a) have a homogeneous size distribution with a diameter of approximately 80 nm. The Pd NPs, which would easily aggregate without MCNs, may grow within the mesoporous channels and on the surface of MCNs. It can be observed (Fig. 2b)

that the Pd NPs on the MCNs surface have a diameter of 5–6 nm. These results indicate that MCNs play a significant role in the *in situ* reduction of Pd^{2+} to form Pd NPs. The composition of hybrid Pd/MCNs was confirmed by energy dispersive X-ray spectroscopy (EDS, inset of Fig. 2b), which revealed the presence of carbon and palladium only with Cu coming from the measurement process. Fig. 3 also presents the hybrid Pd/MCNs XRD pattern, which shows the crystalline nature of Pd NPs in the nanostructures. The diffraction peaks close to 39°, 45°, 67°, and 80° (2θ) can be assigned to the diffraction of palladium (111), (200), (220), and (311).

The amount of palladium in hybrid Pd/MCNs was roughly determined by thermogravimetric analysis (TGA) under air atmosphere at a heating rate of 10 °C/min from 25 to 700 °C. The TGA data shown in Fig. 4 displays the weight loss for the sample and the corresponding derivatives of the weight loss with respect to temperature. The small derivative peak near 100 °C is due to the loss of water in hybrid Pd/MCNs. As the temperature is increased, the functional groups of MCNs in the hybrid are removed as evidenced by the weight loss in the region of 150–300 °C. Another two significant drops in mass are observed around 393 °C and 480 °C, which can be assigned to the carbonization of MCNs. The weight percentage of metal palladium in hybrid Pd/MCNs is estimated to be 16.4%, based upon the amount of residue after TGA.

3.2. Electrochemical behavior of Pd/MCNs modified GCE

The electrocatalytic activity of Pd/MCNs-GCE was investigated by cyclic voltammetry in N_2 saturated PBS (20 mM, pH=7.0) and compared with MCNs modified GCE (MCNs-GCE). As shown in Fig. 5a, the Pd/MCNs-GCE gives one reduction peak in the absence of H_2O_2 at approximately 0 V, which can be attributed to the

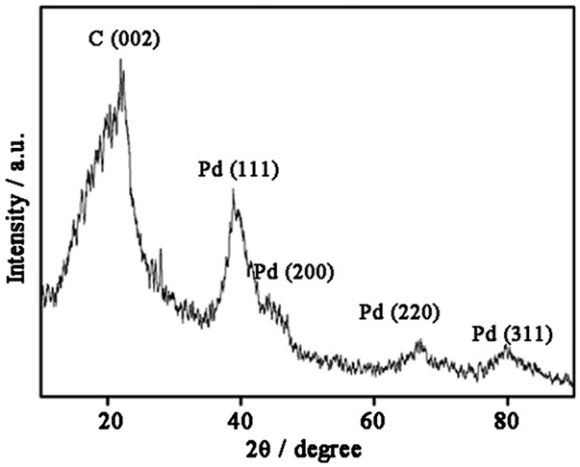

Fig. 3. XRD pattern of hybrid Pd/MCNs.

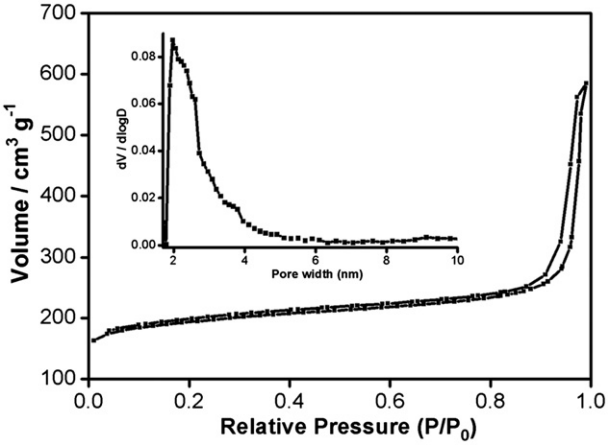

Fig. 1. Nitrogen adsorption/desorption isotherm and DFT pore size distribution (inset) of MCNs.

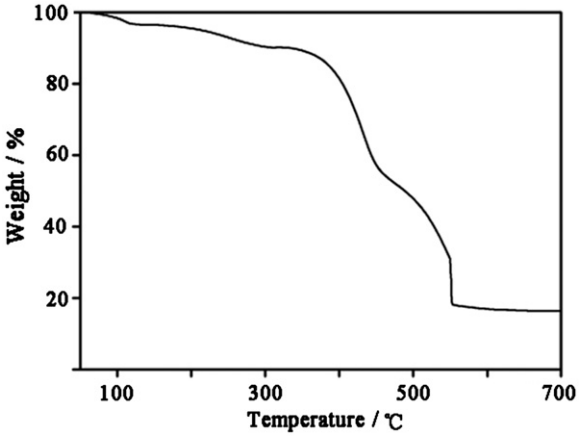

Fig. 4. TGA curve of hybrid Pd/MCNs.

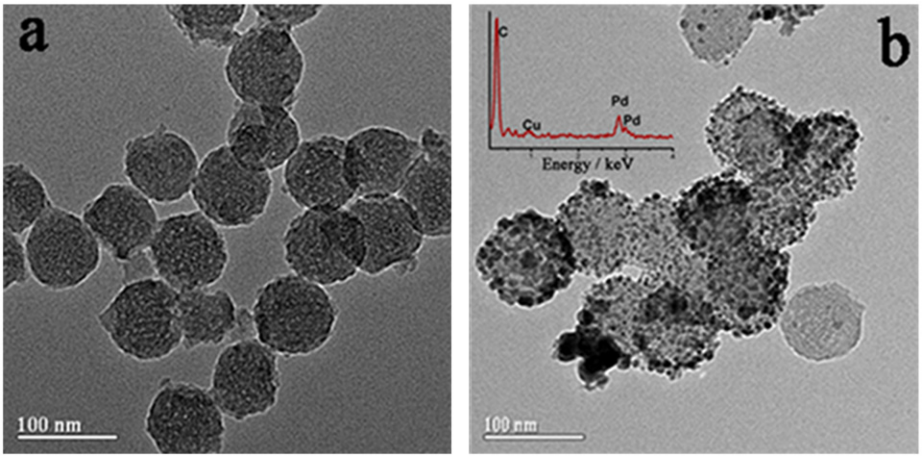

Fig. 2. TEM images of (a) MCNs after acid treatment and (b) hybrid Pd/MCNs with the energy dispersive X-ray spectrum (inset).

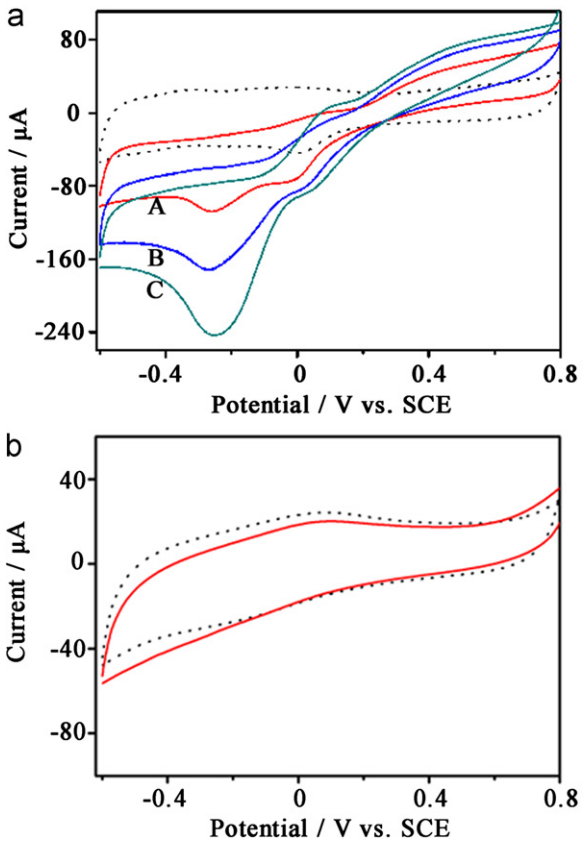

Fig. 5. Cyclic voltammograms of N_2 saturated PBS (20 mM, pH=7.0) (a) in the absence (dotted line) and presence of (A) 1.0 mM, (B) 2.0 mM, and (C) 3.0 mM of H_2O_2 using Pd/MCNs-GCE and (b) in the absence (dotted line) and presence (solid line) of 1.0 mM of H_2O_2 using MCNs-GCE with a scan rate of 20 mV s^{-1}.

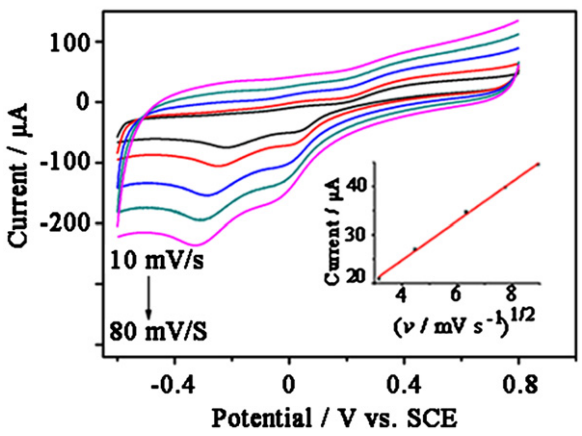

Fig. 6. Cyclic voltammograms for the catalytic reduction of 1.0 mM of H_2O_2 in N_2 saturated PBS (20 mM, pH=7.0) at Pd/MCNs-GCE with different scan rates (10, 20, 40, 60, and 80 mV s^{-1}) and plot of H_2O_2 reduction peak current versus square root of scan rate (inset).

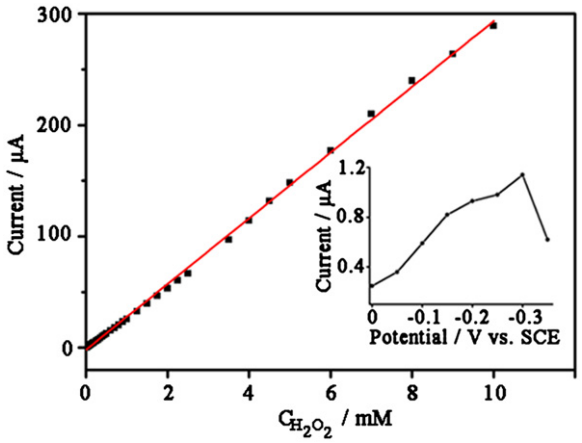

Fig. 7. The amperometric calibration curve for H_2O_2 concentrations between 7.5 μM and 10 mM detected by Pd/MCNs-GCE. Inset is the effect of applied potential on amperometric steady-state current response.

reduction of palladium oxide [38,40]. With the addition of 1.0 mM of H_2O_2, an obvious catalytic reduction peak with relatively high current response can be observed around −0.26 V, which is more positive than some previously reported potentials for nonenzymatic H_2O_2 determination [39,45,46]. Moreover, the reduction peak current increases gradually with the H_2O_2 concentration. In contrast, there is no apparent reduction current change for MCNs-GCE in the presence of 1.0 mM of H_2O_2 (Fig. 5b). According to the literature [47], the reduction of H_2O_2 at Pd/MCNs-GCE can be expressed by the following reaction:

$$H_2O_2 \xrightarrow{Pd/MCNs} H_2O + 1/2O_2$$

The CVs for the catalyzed reduction of H_2O_2 at Pd/MCNs-GCE with different scan rates were also collected. As illustrated in Fig. 6, the cathodic peak currents increase with the scan rates and are proportional to the square roots of scan rates from 10 to 80 mV s^{-1} (inset of Fig. 6), indicating a diffusion controlled electron transfer kinetics for the reduction of H_2O_2 at Pd/MCNs-GCE. Furthermore, it can be observed that the reduction peaks shift slightly to more negative potentials at higher scan rates, demonstrating the electrochemical reduction process for H_2O_2 is irreversible.

3.3. Quantitative determination of H_2O_2

The performance of Pd/MCNs-GCE for the determination of H_2O_2 was evaluated by amperometric analysis. To obtain the best amperometric signal, the effect of applied potential on the reduction of H_2O_2 at Pd/MCNs-GCE was examined. As shown in the inset of Fig. 7, the steady-state current increases with the applied potential shifting negatively from 0 V to −0.30 V but decays afterwards. Consequently, −0.30 V was selected as the reduction potential for the amperometric measurements in this work.

Fig. 8 depicts the amperometric responses at −0.30 V for the successive addition of various amounts of H_2O_2 to N_2 saturated PBS (20 mM, pH=7.0) using Pd/MCNs-GCE, which responds rapidly. The electrochemical sensor can give the maximum steady-state current within 5 s, indicating that the hybrid Pd/MCNs could efficiently catalyze the reduction of H_2O_2. According to the amperometric responses and the electrode surface area (0.096 cm^2), the sensitivity of Pd/MCNs-GCE is calculated to be 307.5 μA mM^{-1} cm^{-2}, which is higher than some previously reported sensors [17,45,48]. Furthermore, the sensor has a wide linear range from 7.5 μM to 10 mM with a correlation coefficient of 0.999 (Fig. 7) and a detection limit of about 1.0 μM which is at least comparable to some similar types of sensors [17,45,48,49]. The high sensitivity, wide linear range, and low detection limit of this sensor are likely due to the efficient electrocatalytic activity of Pd NPs for H_2O_2 reduction and the distinctive 3D structure of MCNs with high specific surface area and large pore volume. The analytical performance of the sensor is summarized in Table 1 and compared with other nonenzymatic H_2O_2 sensors in terms of sensitivity, detection limit, and linear response range.

3.4. Characteristic properties of the Pd/MCNs-GCE sensor

The selectivity and anti-interference capability of Pd/MCNs-GCE were assessed by amperometry in the presence of $NaNO_3$, $NaNO_2$, glucose, ascorbic acid (AA), uric acid (UA), and dopamine (DA), which are the common interfering substances for the detection of H_2O_2 [50]. Fig. 9 presents the amperometric responses at Pd/MCNs-GCE for the successive addition of 0.10 mM of H_2O_2 (twice), 0.10 mM of $NaNO_3$, 0.10 mM of $NaNO_2$, 5.0 mM of glucose, 0.15 mM of AA, 0.35 mM of UA, 0.10 mM of DA, and 0.10 mM of H_2O_2. These concentrations were chosen since the level of endogenous AA, glucose, and UA are approximately 0.125 mM, 4.4 to 6.6 mM, and 0.33 mM in blood samples, respectively. It can be observed in Fig. 9 that the interferences these species may have on H_2O_2 detection are negligible, suggesting a high selectivity of the Pd/MCNs-GCE. Moreover, interferences that might be caused by some transition metal ions such as Cu(II), Zn(II), and Mn(II) were also studied and the results showed that none of them had obvious effect on the detection of H_2O_2 in our system.

The reproducibility of the Pd/MCNs-GCE was tested by ten repetitive measurements of 1.0 mM of H_2O_2 using the same electrode and the relative standard deviation (RSD) of the current responses was less than 3.8%. The reproducibility for different Pd/MCNs-GCEs was also evaluated by using the amperometric signals for 1.0 mM of H_2O_2 at six sensors and a RSD of 5.2% was obtained. The stability of Pd/MCNs-GCE was examined by successive CV scans for 1.0 mM of H_2O_2 in N_2 saturated phosphate buffer. It was observed that the CV features for the H_2O_2 reduction peak remained the same after 200 cycles. Moreover, the amperometric responses of this H_2O_2 sensor decayed by only 8% when kept at room temperature for 2 weeks, demonstrating its long term stability.

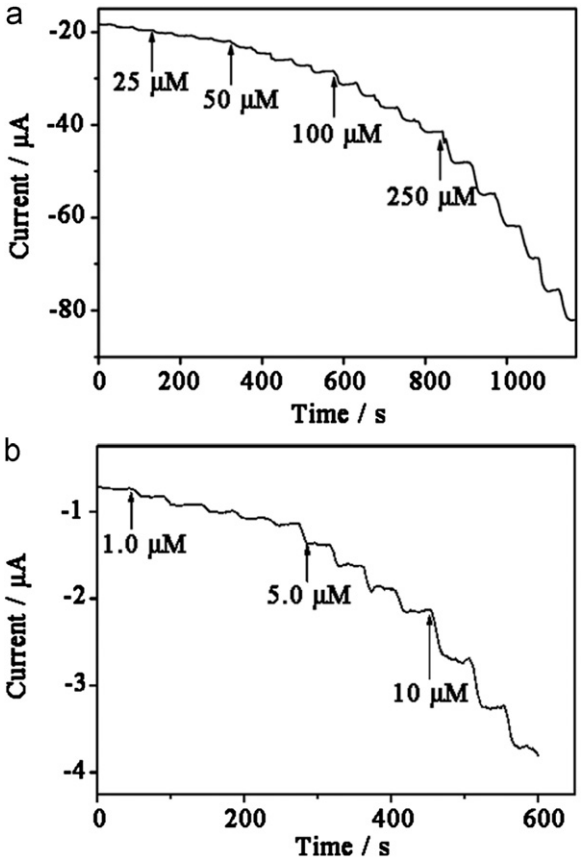

Fig. 8. The amperometric responses (applied potential is −0.3 V) at Pd/MCNs-GCE for successive addition of relatively (a) high and (b) low concentrations of H_2O_2 to N_2 saturated PBS (20 mM, pH=7.0).

4. Conclusion

In summary, a nonenzymatic electrochemical H_2O_2 sensor has been developed based upon a novel matrix of mesoporous carbon nanospheres loaded *in situ* with Pd NPs and this strategy has not been previously reported. The hybrid Pd/MCNs nanocomposites can be used to modify GCE for the detection of H_2O_2. The fabricated sensor gives rapid amperometric response for the catalytic reduction of H_2O_2 with low detection limit (1.0 μM), wide linear range (7.5 μM–10 mM), as well as high sensitivity/selectivity and good stability.

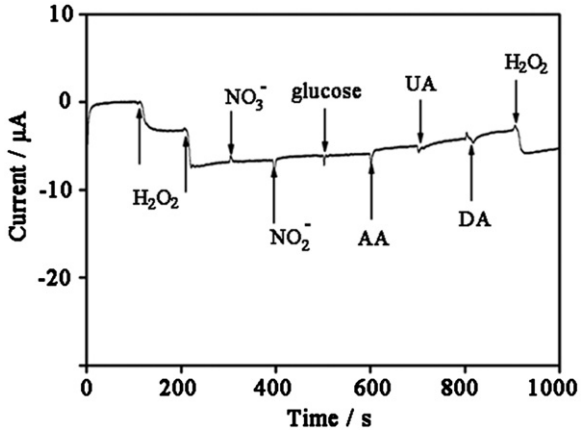

Fig. 9. Amperometric responses at Pd/MCNs-GCE upon successive addition of 0.10 mM of H_2O_2 twice, 0.10 mM of $NaNO_3$, 0.10 mM of $NaNO_2$, 5.0 mM of glucose, 0.15 mM of ascorbic acid (AA), 0.35 mM of uric acid (UA), 0.10 mM of dopamine (DA), and 0.10 mM of H_2O_2 in N_2 saturated PBS (20 mM, pH=7.0) with applied potential of −0.30 V.

Table 1
Comparison of nonenzymatic H_2O_2 sensors.

Sensor	Applied potential (V)	Sensitivity (μA mM^{-1} cm^{-2})	Linear range	Detection limit (μM)	Reference
Pd/MCNs	−0.3	307.5	7.5 μM–10 mM	1.0	This work
Ag/MWCNTs	−0.2		50 μM–17 mM	0.5	[50]
Pt/NAE	−0.65	194.6	20 μM–20 mM	1.0	[49]
Ag/Fe_3O_4	−0.5		1.2 μM–3.5 mM	1.2	[46]
MnO_2/GO	−0.3	38.2	5.0 μM–0.6 mM	1.4	[16]
PDDA-G/Fe_3O_4	−0.4	61.2	20 μM–6.25 mM	2.5	[45]
Pd/TiO_2	−0.2	226.72		3.81	[48]

MCNs=mesoporous carbon nanospheres; MWCNTs=multi-wall carbon nanotubes; NAE=nanowire arrays electrode; GO=graphene oxide; PDDA=polydiallyldimethylammonium; G=graphene.

Acknowledgment

This work was supported by NSFC (20925517, 21175028), SKLEAC201101, and Texas State University Faculty Development Leave Program.

References

[1] W.A.M. Drabkova, B. Marsalek, Environ. Sci. Technol. 41 (2007) 309–314.
[2] L.B. Poole, K.J. Nelson, Curr. Opin. Chem. Biol. 12 (2008) 18–24.
[3] O.S. Wolfbeis, A. Durkop, M. Wu, Z.H. Lin, Angew. Chem. Int. Ed. 41 (2002) 4495–4498.
[4] B.W.J. Jia, A. Wu, G. Cheng, Z. Li, S. Dong, Anal. Chem. 74 (2002) 2217–2223.
[5] E.C. Hurdis, H. Romeyn Jr., Anal. Chem. 26 (1954) 320–325.
[6] S. Hanaoka, J.M. Lin, M. Yamada, Anal. Chim. Acta 426 (2001) 57–64.
[7] L.S. Zhang, G.T.F. Wong, Talanta 48 (1999) 1031–1038.
[8] C. Matsubara, N. Kawamoto, K. Takamura, Analyst 117 (1992) 1781–1784.
[9] J.M. You, Y.N. Jeong, M.S. Ahmed, S.K. Kim, H.C. Choi, S. Jeon, Biosens. Bioelectron. 26 (2011) 2287–2291.
[10] K. Guo, Y. Hu, Y. Zhang, B. Liu, E. Magner, Langmuir 26 (2010) 9076–9081.
[11] Q. Xu, X. Bian, L. Li, X.Y. Hu, M. Sun, C. Da, Y. Wang, Electrochem. Commun. 10 (2008) 995–999.
[12] C. You, X. Yan, J. Kong, D. Zhao, B. Liu, Electrochem. Commun. 10 (2008) 1864–1867.
[13] S.H. Chen, R. Yuan, Y.Q. Chai, L.Y. Zhang, N. Wang, X.L. Li, Biosens. Bioelectron. 22 (2007) 1268–1274.
[14] X. Chen, C. Li, Y. Liu, Z. Du, S. Xu, L. Li, M. Zhang, T. Wang, Talanta 77 (2008) 37–41.
[15] X. Bo, J. Bai, B. Qi, L. Guo, Biosens. Bioelectron. 28 (2011) 77–83.
[16] Y. Ye, T. Kong, X. Yu, Y. Wu, K. Zhang, X. Wang, Talanta 89 (2012) 417–421.
[17] L. Li, Z. Du, S. Liu, Q. Hao, Y. Wang, Q. Li, T. Wang, Talanta 82 (2010) 1637–1641.
[18] X. Huang, W. Wei, X. Zhao, X. Tang, Chem. Commun. 46 (2010) 8848–8850.
[19] D. Long, W. Li, W. Qiao, J. Miyawaki, S.H. Yoon, I. Mochida, L. Ling, Chem. Commun. 47 (2011) 9429–9431.
[20] M. Rose, Y. Korenblit, E. Kockrick, L. Borchardt, M. Oschatz, S. Kaskel, G. Yushin, Small 7 (2011) 1108–1117.
[21] C. You, X. Yan, J. Kong, D. Zhao, B. Liu, Talanta 83 (2011) 1507–1514.
[22] L. Guo, X. Cui, Y. Li, Q. He, L. Zhang, W. Bu, J. Shi, Chem. Asian J. 4 (2009) 1480–1485.
[23] H. Itoi, H. Nishihara, T. Kogure, T. Kyotani, J. Am. Chem. Soc. 133 (2011) 1165–1167.
[24] Y. Zhai, Y. Dou, D. Zhao, P.F. Fulvio, R.T. Mayes, S. Dai, Adv. Mater. 23 (2011) 4828–4850.
[25] J.Y. Kim, S.B. Yoon, J.S. Yu, Chem. Mater. 15 (2003) 1932–1934.
[26] K.G. Lee, J.S. Min, R. Wi, J.C. Kim, J.K. Ahn, D.H. Kim, J. Nanosci. Nanotechnol. 11 (2011) 666–670.
[27] J. Zhang, Y. Zhang, S. Lian, Y. Liu, Z. Kang, S.T. Lee, J. Colloid. Interface Sci. 361 (2011) 503–508.
[28] T.I. Abdullin, O.V. Bondar, Y.G. Shtyrlin, M. Kahraman, M. Culha, Langmuir 26 (2010) 5153–5159.
[29] L.O. Brown, S.K. Doorn, Langmuir 24 (2008) 2277–2280.
[30] V. Mazumder, M. Chi, M.N. Mankin, Y. Liu, O. Metin, D. Sun, K.L. More, S. Sun, Nano Lett. 12 (2012) 1102–1106.
[31] S.H. Won, S.J. Sim, Analyst 137 (2012) 1241–1246.
[32] A. Mehri, H. Kochkar, S. Daniele, V. Mendez, A. Ghorbel, G. Berhault, J. Colloid. Interface Sci. 369 (2012) 309–316.
[33] S. Yasar, E.O. Ozcan, N. Gurbuz, B. Cetinkaya, I. Ozdemir, Molecules 15 (2010) 649–659.
[34] W.P. Zhou, A. Lewera, R. Larsen, R.I. Masel, P.S. Bagus, A. Wieckowski, J. Phys. Chem. B 110 (2006) 13393–13398.
[35] Z.Y. Zhou, X. Kang, Y. Song, S. Chen, Chem. Commun. 47 (2011) 6075–6077.
[36] M. Shao, P. Liu, J. Zhang, R. Adzic, J. Phys. Chem. B 111 (2007) 6772–6775.
[37] M. Shao, T. Yu, J.H. Odell, M. Jin, Y. Xia, Chem. Commun. 47 (2011) 6566–6568.
[38] J. Huang, D. Wang, H. Hou, T. You, Adv. Funct. Mater. 18 (2008) 441–448.
[39] L. Kong, X. Lu, X. Bian, W. Zhang, C. Wang, Langmuir 26 (2010) 5985–5990.
[40] J. Liu, W. Zhou, T. You, F. Li, E. Wang, S. Dong, Anal. Chem. 68 (1996) 3350–3353.
[41] L. Meng, J. Jin, G. Yang, T. Lu, H. Zhang, C. Cai, Anal. Chem. 81 (2009) 7271–7280.
[42] Q. Zeng, J.S. Cheng, X.F. Liu, H.T. Bai, J.H. Jiang, Biosens. Bioelectron. 26 (2011) 3456–3463.
[43] Y. Fang, D. Gu, Y. Zou, Z. Wu, F. Li, R. Che, Y. Deng, B. Tu, D. Zhao, Angew. Chem. Int. Ed. 49 (2010) 7987–7991.
[44] C. You, X. Xu, B. Tian, J. Kong, D. Zhao, B. Liu, Talanta 78 (2009) 705–710.
[45] X. Liu, H. Zhu, X. Yang, Talanta 87 (2011) 243–248.
[46] Z. Liu, B. Zhao, Y. Shi, C. Guo, H. Yang, Z. Li, Talanta 81 (2010) 1650–1654.
[47] X. Bo, J. Bai, J. Ju, L. Guo, Anal. Chim. Acta 675 (2010) 29–35.
[48] L. Kong, X. Lu, X. Bian, W. Zhang, C. Wang, J. Solid State Chem. 183 (2010) 2421–2425.
[49] M. Jamal, J. Xu, K.M. Razeeb, Biosens. Bioelectron. 26 (2010) 1420–1424.
[50] W. Zhao, H. Wang, X. Qin, X. Wang, Z. Zhao, Z. Miao, L. Chen, M. Shan, Y. Fang, Q. Chen, Talanta 80 (2009) 1029–1033.